

Inertial particles in superfluid turbulence: Coflow and counterflow

Cite as: Phys. Fluids **35**, 015153 (2023); <https://doi.org/10.1063/5.0129767>

Submitted: 07 October 2022 • Accepted: 03 January 2023 • Accepted Manuscript Online: 03 January 2023 • Published Online: 24 January 2023

 Sanjay Shukla, Akhilesh Kumar Verma, Vishwanath Shukla, et al.



View Online



Export Citation



CrossMark

ARTICLES YOU MAY BE INTERESTED IN

[Tip vortex cavitation suppression and parametric study of an elliptical hydrofoil by water injection](#)

Physics of Fluids **35**, 013338 (2023); <https://doi.org/10.1063/5.0130192>

[Effects of stabilizing and destabilizing thermal gradients on reversed shear-stratified flows: Combined Kelvin–Helmholtz Rayleigh–Taylor instability](#)

Physics of Fluids **35**, 012118 (2023); <https://doi.org/10.1063/5.0135692>

[An open source package to perform basic and advanced statistical analysis of turbulence data and other complex systems](#)

Physics of Fluids **34**, 101801 (2022); <https://doi.org/10.1063/5.0107974>



Physics of Fluids

Special Topic: Paint and Coating Physics

Submit Today!

Inertial particles in superfluid turbulence: Coflow and counterflow

Cite as: Phys. Fluids **35**, 015153 (2023); doi: 10.1063/5.0129767

Submitted: 7 October 2022 · Accepted: 3 January 2023 ·

Published Online: 24 January 2023








View Online



Export Citation



CrossMark

Sanjay Shukla,^{1,a)}  Akhilesh Kumar Verma,^{2,b)}  Vishwanath Shukla,^{3,c)}  Akshay Bhatnagar,^{4,d)} 
and Rahul Pandit^{1,e)} 

AFFILIATIONS

¹Centre for Condensed Matter Theory, Department of Physics, Indian Institute of Science, Bangalore 560012, India

²Mathematics Institute, Zeeman Building, University of Warwick, Coventry CV4 7AL, United Kingdom

³Department of Physics, Indian Institute of Technology Kharagpur, Kharagpur 721 302, India

⁴Department of Engineering Mechanics, SeRC (Swedish e-Science Research Centre) and Flow, KTH, SE-10044 Stockholm, Sweden

^{a)} Author to whom correspondence should be addressed: ssanjay@iisc.ac.in

^{b)} Electronic address: akvermajnusps@gmail.com

^{c)} Electronic address: vishwanath.shukla@phy.iitkgp.ac.in

^{d)} Electronic address: akshayphy@gmail.com

^{e)} Electronic address: rahul@iisc.ac.in

ABSTRACT

We use pseudospectral direct numerical simulations to solve the three-dimensional (3D) Hall–Vinen–Bekharevich–Khalatnikov (HVBK) model of superfluid helium. We then explore the statistical properties of inertial particles, in both coflow and counterflow superfluid turbulence (ST) in the 3D HVBK system; particle motion is governed by a generalization of the Maxey–Riley–Gatignol equations. We first characterize the anisotropy of counterflow ST by showing that there exist large vortical columns. The light particles show confined motion as they are attracted toward these columns, and they form large clusters; by contrast, heavy particles are expelled from these vortical regions. We characterize the statistics of such inertial particles in 3D HVBK ST: (1) The mean angle $\Theta(\tau)$ between particle positions, separated by the time lag τ , exhibits two different scaling regions in (a) dissipation and (b) inertial ranges, for different values of the parameters in our model; in particular, the value of $\Theta(\tau)$, at large τ , depends on the magnitude of U_m . (2) The irreversibility of 3D HVBK turbulence is quantified by computing the statistics of energy increments for inertial particles. (3) The probability distribution function (PDF) of energy increments is of direct relevance to recent experimental studies of irreversibility in superfluid turbulence; we find, in agreement with these experiments, that, for counterflow ST, the skewness of this PDF is less pronounced than its counterparts for coflow ST or for classical fluid turbulence.

Published under an exclusive license by AIP Publishing. <https://doi.org/10.1063/5.0129767>

I. INTRODUCTION

Over the past few decades, there has been growing interest in studies of the statistical properties of particles advected by turbulent fluid flows, especially because of advances in experimental techniques and computational resources. Such particle advection is of central importance in geophysical^{1–3} and astrophysical⁴ flows, industrial process,^{5,6} nonequilibrium statistical mechanics,⁷ and the visualization of turbulent flows in quantum fluids.^{8–21} However, investigations of particles in turbulent superfluids are in their infancy, when we compare them with their classical fluid turbulence counterparts. Some experimental groups^{14–22} have used particles to visualize vortex lines in superfluid turbulence. In some cases, the particles (e.g., frozen hydrogen or deuterium) are several orders of magnitude larger than the core

size of a vortex. Some of these particles can be modeled as neutrally buoyant tracer particles in superfluid turbulence.

Superfluid turbulence is a multiscale problem for which we must use different levels of description, depending on the length scales that we consider:^{11–13} The Gross–Pitaevskii equation (GPE)^{11,23,24} provides a natural description for a low-temperature, weakly interacting Bose gas, at length scales comparable to the size of the superfluid vortex core, which has a healing length ξ . The vortex-filament model distinguishes between individual quantum vortices, but it does not account for the nature of the vortex core; it is valid on length scales greater than ξ , in the incompressible limit. The Hall–Vinen–Bekharevich–Khalatnikov (HVBK) two-fluid model does not resolve individual quantum vortices but uses macroscopic, classical vorticity fields

(this assumes local polarization of the quantum-vortex lines). At the level of the kinetic theory, there is the model of Zaremba *et al.*²⁵ Some groups have begun to investigate the interactions of classical particles with vortices in a GPE description of superfluid turbulence.^{26–31} These particles are active in the sense that they affect the superfluid flow while they are advected by this flow.

Within the HVBK framework, we can consider both coflow and counterflow superfluid turbulence (ST). In coflow ST, the two fluids move in the same direction, with the same mean velocities; in counterflow ST, superfluid and normal-fluid components move in opposite directions because of an imposed temperature gradient. The statistical properties of counterflow ST are different from those of classical fluid turbulence³² and coflow ST.^{33–35} In counterflow-ST experiments, there is a steady flow along a channel that is closed at one end and open at the other end; a heat flux q is generated by passing a current through a resistor, at the closed end; the normal fluid, which carries this heat flux, with velocity $\mathbf{U}_n = q/\rho ST$, entropy per unit mass S , and at temperature T , moves away from the closed end; to maintain zero mass flux, $\rho_s \mathbf{U}_s + \rho_n \mathbf{U}_n = 0$, so the superfluid flows in the opposite direction, toward the closed end, with velocity $\mathbf{U}_s = -(\rho_n/\rho_s)\mathbf{U}_n$. Thus, there is a relative velocity $\mathbf{U}_{ns} = \mathbf{U}_n - \mathbf{U}_s$ between the two fluids in such thermally driven counterflow ST³⁶

$$\mathbf{U}_{ns} = \frac{\rho}{\rho_s} \mathbf{U}_n, \quad (1)$$

where ρ_n and ρ_s are the densities of the normal-fluid and the superfluid component, respectively, and $\rho = \rho_n + \rho_s$ is the total density. So long as the heat flux q is small, this counterflow is laminar, but if q increases beyond a critical value, this flow is turbulent.

We carry out a systematic study of inertial particles in 3D HVBK coflow ST and counterflow ST.^{40–43} This model has been studied, without particles, for superfluid ⁴He in both two dimensions (2D) and 3D;^{44–47} moreover, a recent study³⁷ has investigated the clustering of inertial particles in 3D HVBK turbulence. Below the critical temperature $T_c = 2.17$ K, superfluid ⁴He is thought of as comprising a viscous, normal-fluid component and an inviscid superfluid component. The density ratio of the normal-fluid component and the total fluid (ρ_n/ρ) is equal to one at T_c and ρ_n/ρ decreases as we decrease the temperature T ; at $T=0$, the normal-fluid component vanishes, and ⁴He is completely in the superfluid form. For $0 < T < T_c$, the normal-fluid component interacts with quantized vortices of the superfluid, via mutual friction;⁴⁸ this causes dissipation in the superfluid component. In this study, we consider inertial particles, whose size is smaller than the Kolmogorov dissipation length of the normal fluid; we assume that these particles are passive insofar as they do not affect the flow and their turbulence-induced accelerations are much larger than the acceleration because of gravity.

We use pseudospectral direct numerical simulations (DNSs) to solve a simplified version of the 3D HVBK model, with inertial particles, whose statistical properties we then study for different values of the mutual-friction coefficients, in this model, and for various values of the Stokes numbers ($St = \tau_p/\tau_f$, where τ_p is the particle-response time, and τ_f is the Kolmogorov-dissipation timescale of the fluid). Inertial particles are different from Lagrangian tracer particles, which follow the fluid velocity; because of their inertia, particles cluster for $St \simeq 1$.^{37,49,50} We summarize our principal results before we present the details of our work:

1. We characterize the anisotropy of counterflow ST by using spectra³⁵ and the anisotropy tensor (see below); we then calculate particle statistics by employing the measures given below.
2. We define persistence times, based on the velocity-gradient tensors of the normal fluid and the superfluid, and show that the cumulative probability distribution functions (CPDFs) of these persistence times have exponential tails in different regions of the flow.
3. The mean angle $\Theta(\tau)$, between particle positions separated by the time lag τ (defined precisely below), has two different scaling regions (in dissipation and inertial ranges) for different values of the Stokes numbers and the mutual-friction coefficients.
4. The CPDFs of the curvature κ and the modulus θ of the torsion of particle trajectories have power-law tails with universal exponents, which are independent of all the control parameters in our model.
5. We characterize the irreversibility of 3D HVBK turbulence, by using inertial particles, and quantify its dependence on the Stokes numbers.

The remainder of this paper is organized as follows. We describe the HVBK model and our DNSs in Sec. II. We present, in Sec. III, the details of our results. We discuss the implications of our results in the concluding Sec. IV.

II. MODEL AND NUMERICAL SIMULATIONS

We use the simplified form of the 3D HVBK equations.⁴⁴ In addition to the kinematic viscosity ν_n of the normal fluid, we include Vinen's effective viscosity⁵¹ ν_s in the superfluid component to mimic the dissipation because of (a) vortex reconnections and (b) interactions between superfluid vortices and the normal fluid;⁵² the equations for this simplified, incompressible 3D HVBK model (we use the form suggested in Ref. 33) for fluctuations \mathbf{u}_n and \mathbf{u}_s with zero mean are

$$\begin{aligned} \partial_t \mathbf{u}_n + [(\mathbf{u}_n + \mathbf{U}_n) \cdot \nabla] \mathbf{u}_n &= -\frac{1}{\rho_n} \nabla p_n + \nu_n \nabla^2 \mathbf{u}_n + \mathbf{F}_{mf}^n + \mathbf{f}_n, \\ \partial_t \mathbf{u}_s + [(\mathbf{u}_s + \mathbf{U}_s) \cdot \nabla] \mathbf{u}_s &= -\frac{1}{\rho_s} \nabla p_s + \nu_s \nabla^2 \mathbf{u}_s + \mathbf{F}_{mf}^s + \mathbf{f}_s. \end{aligned} \quad (2)$$

Here, $\mathbf{u}_n(\mathbf{u}_s)$, $\mathbf{U}_n(\mathbf{U}_s)$, $\rho_n(\rho_s)$, $p_n(p_s)$, and $\nu_n(\nu_s)$ are the velocity, mean velocity, density, pressure, and kinematic viscosity of the normal fluid (superfluid), respectively; \mathbf{U}_n and \mathbf{U}_s vanish for coflow but not for counterflow. The mean relative velocity $\mathbf{U}_{ns} = \mathbf{U}_n - \mathbf{U}_s$ is non-zero for counterflow, and it cannot be eliminated by a Galilean transformation as discussed in Ref. 34. The mutual-friction terms \mathbf{F}_{mf}^n and \mathbf{F}_{mf}^s , which lead to energy transfer between normal-fluid and superfluid components,^{53,54} are

$$\begin{aligned} \mathbf{F}_{mf}^s &= -\frac{\rho_n}{\rho} \mathbf{f}_{mf}; & \mathbf{F}_{mf}^n &= \frac{\rho_s}{\rho} \mathbf{f}_{mf}; \\ \mathbf{f}_{mf} &= \frac{B}{2} \hat{\omega}_s \times (\omega_s \times (\mathbf{u}_n - \mathbf{u}_s)) + \frac{B'}{2} \omega_s \times (\mathbf{u}_n - \mathbf{u}_s), \end{aligned} \quad (3)$$

where $\rho = \rho_n + \rho_s$ is the total density, $\mathbf{u}_{ns} = \mathbf{u}_n - \mathbf{u}_s$ is the slip velocity, $\omega_s = \nabla \times \mathbf{u}_s$ is the superfluid vorticity, B and B' are the mutual-friction coefficients, and \mathbf{f}_n and \mathbf{f}_s are the external forcing terms for the normal fluid and superfluid, respectively, and the caret denotes a unit vector. We consider incompressible flows for which we use the incompressibility conditions

$$\nabla \cdot \mathbf{u}_n = 0 \quad \text{and} \quad \nabla \cdot \mathbf{u}_s = 0, \quad (4)$$

for the normal fluid and the superfluid, respectively. Given these incompressibility conditions, the pressures p_n and p_s can be eliminated from the equations; if these pressures are required, we can calculate them by using the Poisson equations that relate them to the velocity fields, but we do not need them in this study. We carry out a Fourier-pseudospectral DNS study of the 3D HVBK equations (2) and (4) by using the following:

- a cubical box of side 2π , with periodic boundary conditions along each direction, N^3 collocation points, and the 2/3 dealiasing rule.⁵⁵
- in this pseudospectral method,^{23,56} the derivatives in Eq. (2) are evaluated in Fourier space where they are local, and products are evaluated in physical space; for Fast Fourier transforms (FFT) and their inverses, we use the FFTW⁵⁷ libraries;
- the constant-energy-injection scheme^{58,59} is used to force the Fourier modes, which lie in the first two shells in Fourier space, for both the normal fluid and the superfluid;
- the second-order Adams–Bashforth scheme for time marching.⁵⁹
- In our direct numerical simulations (DNSs), we use smooth initial conditions; furthermore, the flow is incompressible, so there are no shocks. Of course, we do use 2/3 dealiasing, as we have mentioned in our paper; we have checked explicitly, by using two resolutions, namely, $N^3 = 256^3$ and $N^3 = 512^3$ that the statistical properties we consider are not affected significantly by this change of resolution.

The parameters for our DNSs are given in Table I; here, $Re_\lambda^n (Re_\lambda^s)$, $\tau_{eddy}^n (\tau_{eddy}^s)$, $\eta_n (\eta_s)$, $\tau_\eta^n (\tau_\eta^s)$, and T are the Taylor-microscale Reynolds number, eddy-turn-over time, Kolmogorov dissipation length and time scales for the normal fluid (superfluid), and temperature (in kelvin), respectively. We use the temperature-dependent values of ρ_n , ρ_s , B , and B' from the experiments of Ref. 60. The values of the viscosities are taken from Ref. 61. We use $\nu_n/\nu_s \leq 10$; it is difficult to go beyond this ratio with the resolution of our DNS. [This is similar to the problem faced by DNSs of magnetohydrodynamics (MHD) turbulence when the magnetic Prandtl number (the ratio of the fluid kinematic viscosity and magnetic diffusivity) is very different from unity.⁵⁹]

TABLE I. Parameters for our DNS runs. Coflow ST: R1–R3; and counterflow ST: R4–R8. N^3 is the total number of collocation points; ρ_n/ρ is the normal-fluid fraction; the non-dimensionalized counterflow velocity $\tilde{U}_{ns} = |\mathbf{U}_{ns}|/u_T^n$, where $u_T^n = \sqrt{\langle |\mathbf{u}_n|^2 \rangle}$ and the angular brackets denote the average over the turbulent, but statistically steady state of the 3D HVBK system; B and B' are the coefficients of mutual friction; $\nu_n (\nu_s)$, $Re_\lambda^n (Re_\lambda^s)$, $\tau_{eddy}^n (\tau_{eddy}^s)$, $\eta_n (\eta_s)$, $\tau_\eta^n (\tau_\eta^s)$, and T are the kinematic viscosity, Taylor-microscale Reynolds number, eddy-turn-over time, Kolmogorov dissipation length and time scales for the normal fluid (superfluid), and temperature (in kelvin), respectively; the time step is dt ; k_{max} is the largest wave number (after dealiasing); and $f_n (f_s)$ provide constant energy injection into the first two shells in Fourier space for the normal fluid (superfluid); we force both the fluids.

Run	N	T	ρ_n/ρ	\tilde{U}_{ns}	B	B'	$\nu_n/10^4$	$\nu_s/10^4$	$dt/10^4$	f_n	f_s	Re_λ^n	Re_λ^s	τ_{eddy}^n	τ_{eddy}^s	$k_{max}\eta_n$	$k_{max}\eta_s$	τ_η^n	τ_η^s
R1	256	1.65	0.193	0.00	1.14	0.15	11.3	2.3	10	0.02	0.02	34	124	1.43	1.34	1.26	0.46	0.19	0.13
R2	256	2.10	0.741	0.00	1.30	-0.07	1.67	10	10	0.02	0.02	153	40	1.30	1.41	0.36	1.14	0.11	0.18
R3	512	1.65	0.193	0.00	1.14	0.15	11.3	2.3	8	0.02	0.02	35	211	1.24	1.14	2.04	0.49	0.15	0.09
R4	256	1.65	0.193	11.32	1.14	0.15	11.3	2.3	10	0.02	0.02	287	758	1.60	1.45	2.45	0.68	0.58	0.29
R5				20.31								237	561	1.90	1.65	2.46	0.71	0.74	0.31
R6	256	2.10	0.741	8.94	1.30	-0.07	1.67	10	10	0.02	0.02	374	177	1.82	2.10	0.50	2.14	0.21	0.63
R7	512	1.65	0.193	12.90	1.14	0.15	11.3	2.3	8	0.02	0.02	58	244	4.32	2.51	6.22	1.77	1.17	0.47
R8	512	2.10	0.741	8.54	1.30	-0.07	1.7	10.0	8	0.02	0.02	190	62	2.17	4.12	1.13	5.40	0.26	1.00

To study the advection of inertial particles in this HVBK model, we consider that (a) the radius of the particles $a \ll \eta_n$, where η_n is the Kolmogorov dissipation length scales for normal fluid, (b) particles do not interact with each other, (c) particles do not affect the fluid flows, and (d) turbulence-induced particle accelerations are much greater than the acceleration because of gravity. The particle's radius $\simeq 1 \rightarrow 5 \times 10^{-3}$ cm, and the Kolmogorov length scale for the normal fluid at $T = 1.65K$ is $\simeq 1 \times 10^{-2}$ cm. Under these conditions, the evolution equations for the particles, discussed in Refs. 62–64 for a classical fluid, can be generalized, in the HVBK model,¹⁶ to

$$\frac{d\mathbf{v}(t)}{dt} = \frac{\mathbf{u}_n(\mathbf{X}, t) - \mathbf{v}(t)}{\tau_p} + \beta \left(\frac{\rho_n D\mathbf{u}_n}{\rho Dt} + \frac{\rho_s D\mathbf{u}_s}{\rho Dt} \right) \quad (5)$$

$$\frac{d\mathbf{X}(t)}{dt} = \mathbf{v}(t);$$

here, $\mathbf{v}(t)$ and $\mathbf{X}(t)$ are, respectively, the velocity and position of the particle at time t ; and $\mathbf{u}_n(\mathbf{X}, t)$ and $\mathbf{u}_s(\mathbf{X}, t)$ are the Eulerian normal-fluid and superfluid velocities at position \mathbf{X} and time t ; D/Dt is the material derivative; the term with the coefficient

$$\beta \equiv 3\rho/(2\rho_p + \rho), \quad (6)$$

accounts for added-mass effects (ρ_p is the particle's density); the particle-response time for the normal fluid is

$$\tau_p = \frac{a^2 \rho}{3\beta \rho_n \nu_n}. \quad (7)$$

To study the statistical properties of such particles, we solve Eq. (5) for (a) $N_p = 100\,000$ particles, by using the first-order Euler scheme for time marching and tri-linear interpolation, to calculate the particles' velocities at off-grid points, and (b) for different Stokes numbers

$$St_n = \frac{\tau_p}{\tau_n}, \quad (8)$$

with $\tau_n = (\nu_n/\epsilon_n)^{1/2}$ the Kolmogorov timescale for the normal fluid, and ϵ_n is the rate of kinetic energy dissipation for the normal fluid; the higher these Stokes numbers, the higher the particle inertia.

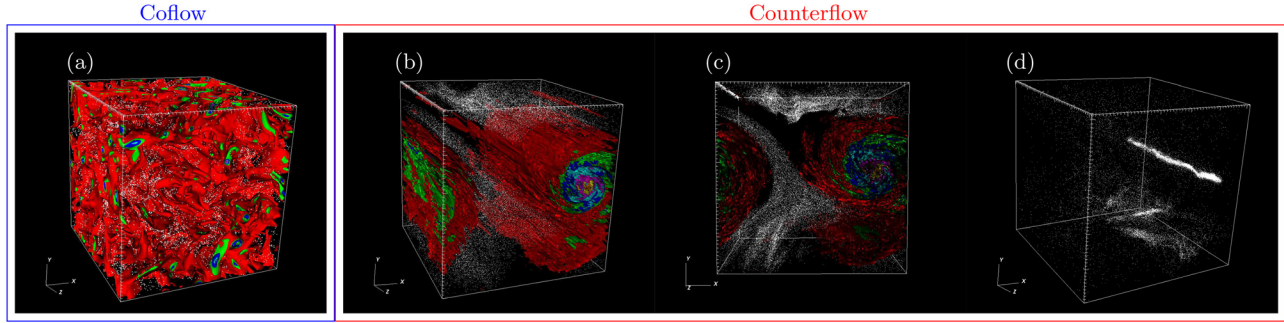


FIG. 1. Isosurface plots of the magnitude of the normal-fluid vorticity $|\omega_n|$ with particles as white points, at $T = 1.65$ K. (a) Coflow ST (R1) and (b)–(d) counterflow ST (R5); (c) a 2D view of (b) for heavy particles ($\beta = 0.1$); and (d) the same plot as in (c) but for light particles ($\beta = 1.25$). The counterflow velocity is along the z direction, which points out of the page in (c).

III. RESULTS

We study the statistics of inertial particles for different values of St_n and β in the 3D HVBK model for our different DNS runs. Before we discuss these statistics of inertial particles we present, in Fig. 1, isosurface plots of the magnitude of the normal-fluid vorticity $|\omega_n|$ at $T = 1.65$ K: Figs. 1(a)–1(d) show, respectively, such isosurface plots for coflow and counterflow ST; in the latter case, the counterflow velocity points along $\hat{U}_{ns} = \hat{e}_k$, where \hat{e}_k is the unit vector along the z direction. We present isosurfaces for $St_n = 1.0$ and $\beta = 1.25$ ($\rho_p/\rho = 0.7$) and $\beta = 0.1$ ($\rho_p/\rho = 14.5$). For coflow, the spatial organization of isosurfaces appears to be isotropic at $T = 1.65$ K and particles form clusters [Fig. 1(a)] as in classical fluid turbulence. In contrast, counterflow ST exhibits large-scale vortex columns [Fig. 1(b)], in which heavy particles ($\beta = 0.1$) form large clusters [Fig. 1(c)] that are repelled from the regions with large vortical structures; however, light particles ($\beta = 1.25$) are attracted toward these structures [Fig. 1(d)]. In Fig. S1 of supplementary material V, we show isosurface plots of $|\omega_n|$ for counterflow ST at $T = 2.10$ K; the distribution of particles is similar to that at $T = 1.65$ K.

We also characterize the anisotropy of counterflow ST by using the anisotropy tensor a_{ij} and energy spectra. The anisotropy tensor has the components

$$a_{ij} = \frac{\overline{u_i u_j}}{\overline{u_i u_i}} - \frac{1}{3} \delta_{ij}, \quad (9)$$

where u_i and u_j are the Cartesian components of the fluctuating velocity for the normal fluid, we use the Einstein summation convention for repeated indices, and the overbar denotes the volume average. We calculate different off diagonal components of a_{ij} and find, e.g., that $a_{ij} \simeq 10^{-3}$ for coflow ST at $T = 1.65$ K; by contrast, for counterflow ST, $a_{ij} \simeq 2 \times 10^{-1}$. This shows clearly the degree of anisotropy in the counterflow ST in our DNS. Furthermore, we examine the anisotropy of counterflow ST by using the following energy spectra:³⁵

$$E_{k_{\parallel}}^l = \frac{1}{2} \sum_{k_{\parallel} - \frac{1}{2} < k' < k_{\parallel} + \frac{1}{2}} \tilde{\mathbf{u}}_{\parallel}^l(\mathbf{k}') \cdot \tilde{\mathbf{u}}_{\parallel}^l(-\mathbf{k}'), \quad (10)$$

$$E_{k_{\perp}}^l = \frac{1}{2} \sum_{k_{\perp} - \frac{1}{2} < k' < k_{\perp} + \frac{1}{2}} \tilde{\mathbf{u}}_{\perp}^l(\mathbf{k}') \cdot \tilde{\mathbf{u}}_{\perp}^l(-\mathbf{k}'),$$

here, l can be n or s ; we denote by $\tilde{\mathbf{u}}_{\parallel}^l$ and $\tilde{\mathbf{u}}_{\perp}^l$ the spatial Fourier transforms of the velocities in the directions \mathbf{k}_{\parallel} and \mathbf{k}_{\perp} , respectively, where

$\mathbf{k}_{\parallel} = (\mathbf{k} \cdot \hat{U}_{ns}) \hat{U}_{ns}$ and, perpendicular to it, $\mathbf{k}_{\perp} = \mathbf{k} - \mathbf{k}_{\parallel}$; and k' , k_{\parallel} , and k_{\perp} are, respectively, the magnitudes of \mathbf{k}' , \mathbf{k}_{\parallel} , and \mathbf{k}_{\perp} . We plot, in Fig. 2, the energy spectra $E_{k_{\perp}}^n$ (dark blue) and $E_{k_{\parallel}}^n$ (cyan) for the normal-fluid component of counterflow ST at $T = 1.65$ K for $\hat{U}_{ns} = \hat{e}_k$ (run R5). Note that $E_{k_{\parallel}}^n$ is strongly pressed relative to $E_{k_{\perp}}^n$; furthermore, these spectra show two distinct (blue-shaded region) power-law forms that are consistent with $E_{k_{\perp}}^n \sim k_{\perp}^{-8/3}$ and $E_{k_{\parallel}}^n \sim k_{\parallel}^{-11/3}$. These spectra are in agreement with the recent results of Ref. 35.

This anisotropy of counterflow ST affects the trajectories of inertial particles, which are advected by such turbulence. We can visualize this qualitatively by including the positions of, say, 10 000 particles (shown via small white spheres) along with the isosurfaces, in Fig. 1, of the magnitude of the normal-fluid vorticity $|\omega_n|$. Clearly, in the case of counterflow ST at $T = 1.65$ K [Fig. 1(c)], particles form large clusters

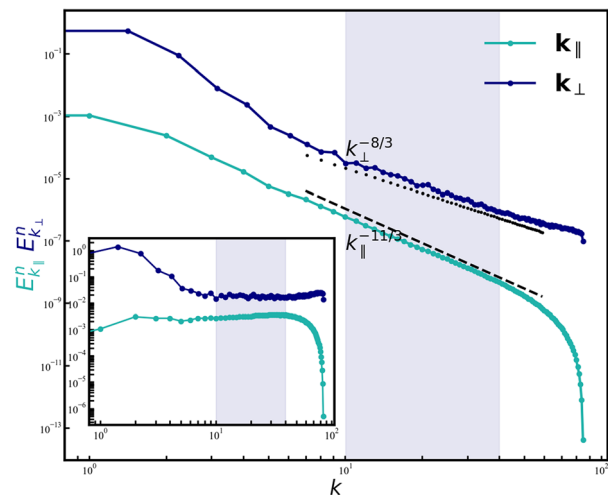


FIG. 2. Log-log plots of the energy spectra [Eq. (10)] $E_{k_{\perp}}^n$ (dark blue) and $E_{k_{\parallel}}^n$ (cyan) for the normal fluid component of counterflow ST with $T = 1.65$ K and $\hat{U}_{ns} = \hat{e}_k$ (run R5). The blue shaded region shows the inertial range of scales. In the inset, we plot the compensated spectra $E_{k_{\perp}}^n * k_{\perp}^{8/3}$ (dark blue) and $E_{k_{\parallel}}^n * k_{\parallel}^{11/3}$ (cyan).

around large vortical structures and move principally along the direction \hat{U}_{ns} of the counterflow velocity.

In Subsection III A, we characterize the flow in the Eulerian frame by using joint PDFs (JPDFs) of the Q and R invariants of the velocity-gradient tensor. In Subsection III B, we obtain the angle Θ that quantifies the statistics of inertial-particle displacement increments. Subsection III C is devoted to a characterization of the statistical properties of the geometry of particle trajectories. In Subsection III D, we characterize the irreversibility of 3D HVBK turbulence. In all these subsections, we compare and contrast our results for coflow ST and counterflow ST; we also examine the dependence of some of the results on the non-dimensionalized counterflow velocity $\tilde{U}_{ns} = |\mathbf{U}_{ns}|/u_T^n$, where $u_T^n = \sqrt{\langle |\mathbf{u}_n|^2 \rangle}$, and the angular brackets denote the average over the turbulent, but statistically steady state of the 3D HVBK system. Figure 9 in the Appendix shows the time series of the volume-averaged energy, $E(t) = \sum_{k_{\parallel}} E_{k_{\parallel}} + \sum_{k_{\perp}} E_{k_{\perp}}$, in the statistically steady state for run R1; here, $E_{k_{\parallel}}$ and $E_{k_{\perp}}$ are defined in Eqs. (10).

A. Joint probability distribution of Q-R invariants

We begin by calculating the invariants P_a , Q_a , and R_a of the velocity-gradient tensor $\mathcal{A}_{aij} = \partial_j u_{ai}$

$$\begin{aligned} P_a &= -\text{Tr}(\mathcal{A}_a), \\ Q_a &= -\frac{1}{2}\text{Tr}(\mathcal{A}_a^2), \\ R_a &= -\frac{1}{3}\text{Tr}(\mathcal{A}_a^3), \end{aligned} \quad (11)$$

where the subscript a stands for n or s , and $i, j = 1, 2, 3$. For incompressible flows, $P_a = 0$. The discriminant for the characteristic equation of \mathcal{A}_a is

$$\Delta_a = \frac{27}{4}R_a^2 + Q_a^3. \quad (12)$$

We use these invariants and Δ_a , in the $Q_a - R_a$ plane, to characterize the following four types of flows regions (for this well-established method, see, e.g., Ref. 74 and references therein):

- Region A: vortical flow with stretching, for $\Delta_a > 0$ and $R_a < 0$;
- Region B: vortical flow with compression, for $\Delta_a > 0$ and $R_a > 0$;
- Region C: flow with biaxial strain, for $\Delta_a < 0$ and $R_a < 0$;
- and Region D: flow with axial strain, for $\Delta_a < 0$ and $R_a > 0$.

Joint PDFs (JPDFs) of Q_a and R_a are often used to characterize turbulent flows in classical fluid turbulence,⁷⁴ where they have a characteristic tear-drop shape, i.e., in strain-dominated regions ($Q < 0$), $R > 0$ is more probable than $R < 0$, whereas the opposite holds in vortical regions ($Q > 0$). In Fig. 3, we present filled contour plots of four representative JPDFs for coflow ST [Figs. 3(a) and 3(b)] and counterflow ST [Figs. 3(c) and 3(d)] at $T = 1.65$ K; these are in the Eulerian frame. The four flow regions, (A)–(D), are shown in Fig. 3(a). We note that the JPDFs for coflow ST have a tear-drop shape, as in classical fluid turbulence; but those for counterflow ST show some deviations from this shape, which means that, in the strain-dominated region ($Q < 0$), both $R < 0$ and $R > 0$ are almost equally probable [and likewise for the vortical region ($Q > 0$)]. Some groups⁷⁵ have found, for various experimental turbulent flows, that the shape of the $Q - R$ JPDF depends on the flow and that deviations from a tear-drop shape may arise if we have vortex-sheet-like structures rather than vortex-tube-like structures; these depend on the sign of the second eigenvalue of strain-rate tensor. We will discuss this in detail, in the context of counterflow ST, elsewhere. In this paper, we focus principally on our particle-based studies.

In each one of these flow regions, (A)–(D), we calculate the PDFs of persistence times t_n^{per} and t_s^{per} for the normal-fluid (n) and superfluid (s) components, respectively. These are the times spent by a particle, in a given region, before it moves to another region (for classical fluid turbulence, see Ref. 74). We calculate persistence-time PDFs in the Eulerian frame, by measurements of Q_a, R_a , and Δ_a , at a fixed point in space, as a function of time t . We get similar PDFs for tracers or inertial particles by following the trajectory of each such particle and obtaining Q_a, R_a , and Δ_a along its trajectory.

In Fig. 4, we present semilog plots of the persistence-time CPDFs at two temperatures ($T = 1.65$ and 2.10 K), in the Eulerian frame, for the normal fluid and for coflow ST in Fig. 4(a) and for counterflow ST in Fig. 4(b). We give similar plots for the superfluid component, in Fig. S2, in supplementary material V. From the semilog plots in Figs. 4 and S2, we observe that, for both coflow and counterflow ST, persistence-time CPDFs (and PDFs) have exponentially decaying tails in all the regions A–D and in both the normal fluid and the superfluid.

B. Inertial-particle displacement increments

In the context of classical fluid turbulence, it has been noted in Ref. 65 that the study of the changes in the direction of Lagrangian tracers reveals two power-law ranges. We carry out the analog of this

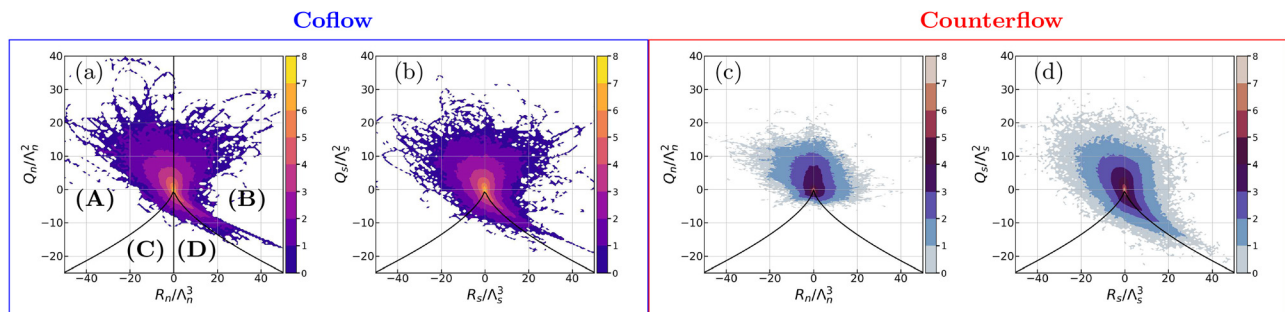


FIG. 3. Filled contour plots of four representative JPDFs for coflow ST [(a) and (b) from run R3] and counterflow ST [(c) and (d) from run R7]; we give JPDFs of Q_n and R_n in the first and third columns and of Q_s and R_s in the second and fourth columns; these are in the Eulerian frame. $\Lambda_n = \frac{U_{ns}}{\eta_n}$ and $\Lambda_s = \frac{U_{ns}}{\eta_s}$.

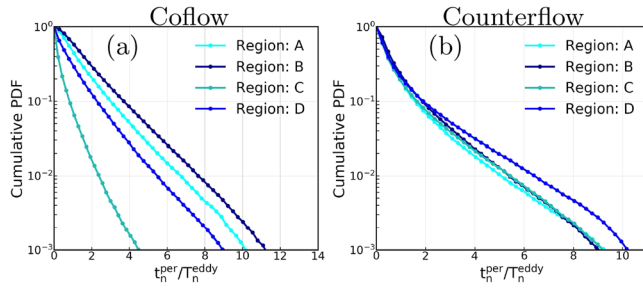


FIG. 4. Semilog plots of the CPDFs of the persistence times, t_n^{per} , at $T = 1.65$ K in the Eulerian frame for the normal-fluid (n) component; for coflow ST (run R3) in (a) and for counterflow ST (run R7) in (b).

analysis for inertial particles advected by 3D HVBK coflow and counterflow ST; our study highlights the effect of \tilde{U}_{ns} on the change in the direction of these particles. From our DNSs, we obtain the angle $\Theta(\tau)$ between subsequent inertial-particle-displacement increments⁶⁵ as a function of the time lag τ as follows:

$$\delta\mathbf{X}(\mathbf{x}_0, t, \tau) = \mathbf{X}(\mathbf{x}_0, t) - \mathbf{X}(\mathbf{x}_0, t - \tau), \quad (13)$$

where $\mathbf{X}(\mathbf{x}_0, t)$ is the position of the particle at time t , and \mathbf{x}_0 is the reference position for the particle at time t_0 . The angle $\Theta(t, \tau)$ is given by

$$\cos(\Theta(t, \tau)) = \frac{\delta\mathbf{X}(\mathbf{x}_0, t, \tau) \cdot \delta\mathbf{X}(\mathbf{x}_0, t + \tau, \tau)}{|\delta\mathbf{X}(\mathbf{x}_0, t, \tau)| |\delta\mathbf{X}(\mathbf{x}_0, t + \tau, \tau)|}, \quad (14)$$

whose average value, over the time t and the number of particles N_p , is

$$\langle \Theta(\tau) \rangle = \langle |\Theta(t, \tau)| \rangle_{t, N_p}. \quad (15)$$

For coflow ST at $T = 1.65$ K [Fig. 5(a)], we present the log–log plot of $\langle \Theta(\tau) \rangle$ vs τ for different values of St_n and $\beta = 1.25$ ($\rho_p/\rho_o = 0.7$). These plots show two power-law scaling regions separated by a crossover regime around τ_n^n , the Kolmogorov timescale: in the dissipation range (cyan-shaded regions) $\langle \Theta(\tau) \rangle \sim \tau^\alpha$; in the inertial range (green-shaded regions) $\langle \Theta(\tau) \rangle \sim \tau^\zeta$; our data are consistent with the exponents $\alpha \simeq 1$ and $\zeta \simeq 1/2$. Similar scaling regimes have been

obtained for Lagrangian tracers in classical fluid turbulence⁶⁵ except at a large Stokes number in which case particles become ballistic and do not show the inertial range. This shows that coflow ST at $T = 1.65$ K or higher temperatures behaves like classical fluid turbulence because the normal-fluid and superfluid components are strongly coupled by the mutual friction.

For counterflow ST at $T = 1.65$ K [Fig. 5(b)], the scaling region in the dissipation range ($\tau < \tau_n^n$) yields $\alpha \simeq 1$, as in coflow ST. Beyond τ_n^n , because of the mean counterflow speed ($\tilde{U}_{ns} = 20.31$), particles form large clusters [Figs. 1(b)–1(d)]. For light particles [Fig. 1(d)], these large clusters are attracted toward the vortex columns and are substantially confined. This confinement reduces the asymptotic value of $\langle \Theta \rangle$ at large τ (as compared to its counterpart in coflow ST). In particular, particles with large St_n [cyan curve in Fig. 5(b)] are strongly affected by this confinement because they follow the normal-fluid component, which has large mean velocity U_n as compared to that of the superfluid component U_s (cf. Ref. 66 for a related effect in classical fluid turbulence). At a higher temperature, say $T = 2.10$ K, the superfluid fraction is very small, and the behavior of $\langle \Theta \rangle$ is similar to that in classical fluid turbulence [Fig. 5(c)] with the scaling exponents $\alpha \simeq 1$ and $\zeta \simeq 1/2$; of course, at large values of τ , $\langle \Theta \rangle$ is reduced, because of the mean counterflow velocity, as it is for $T = 1.65$ K.

C. Particle trajectories

In addition to the statistics of particle velocities and accelerations in coflow and counterflow ST, it is instructive to examine the statistics of the trajectory curvature κ and the modulus θ of the torsion. Both of these quantities have dimensions of inverse length, so large values of κ and θ provide information about small-scale structures. To characterize the geometry of a particle's trajectory, we follow Ref. 67 and use the tangent \mathbf{t} , normal \mathbf{n} , and bi-normal \mathbf{b} that are defined as^{68–70}

$$\mathbf{t} = \frac{d\mathbf{r}}{ds}; \quad \mathbf{n} = \frac{1}{\kappa} \frac{d\mathbf{t}}{ds}; \quad \mathbf{b} = \mathbf{t} \times \mathbf{n}. \quad (16)$$

Here, s is the arc length, and κ is the curvature of the trajectory; \mathbf{t} , \mathbf{n} , and \mathbf{b} evolve as follows:

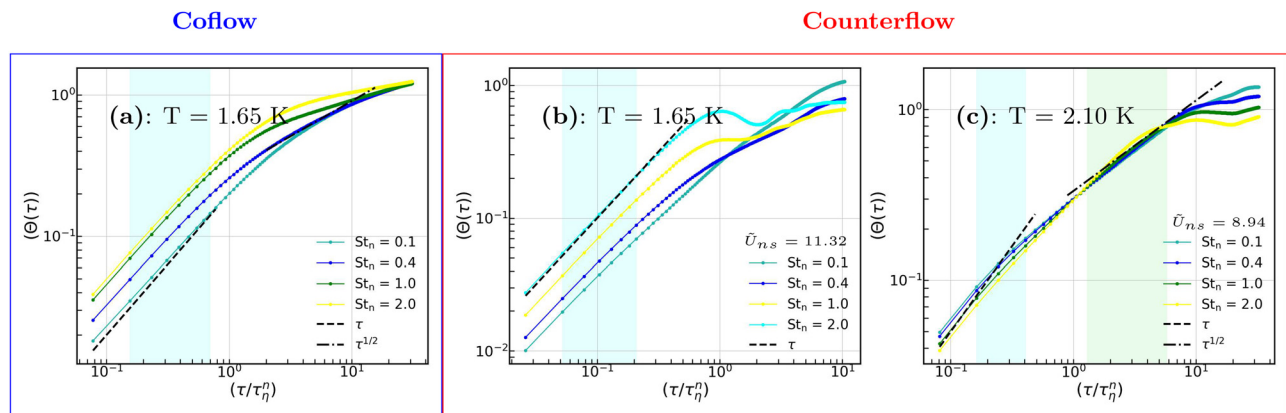


FIG. 5. Log–log plots of the angle $\langle \Theta(\tau) \rangle$ (see the text) vs the time lag τ for (a) coflow ST at $T = 1.65$ K, (b) and (c) counterflow ST at $T = 1.65$ K and $T = 2.1$ K, respectively. These plots are for $\beta = 1.25$ and for different values of St_n . Note the power-law scaling regions in the dissipation ranges (cyan-shaded regions) and in the inertial ranges (green-shaded regions) with $\langle \Theta(\tau) \rangle \sim \tau^\alpha$ and $\langle \Theta(\tau) \rangle \sim \tau^\zeta$, respectively.

$$\frac{dt}{ds} = \kappa \mathbf{n}; \quad \frac{d\mathbf{n}}{ds} = \vartheta \mathbf{b} - \kappa \mathbf{t}; \quad \frac{d\mathbf{b}}{ds} = -\vartheta \mathbf{n}. \quad (17)$$

ϑ is the torsion of the trajectory. In terms of \mathbf{v} and its derivatives $(\dot{\mathbf{v}}, \ddot{\mathbf{v}})$, we have, in parametric form

$$\kappa = \frac{|\mathbf{v} \times \dot{\mathbf{v}}|}{|\mathbf{v}|^3} = \frac{a_n}{v^2}; \quad \vartheta = \frac{\mathbf{v} \cdot (\dot{\mathbf{v}} \times \ddot{\mathbf{v}})}{(\mathbf{v} \cdot \mathbf{v})^3 \kappa^2}. \quad (18)$$

where v and a_n are the magnitude of the velocity and of the normal component of particle's acceleration.

In the log-log plots of Figs. 6(a) and 6(b), we present for coflow ST, the CPDFs $Q(\kappa)$ and $Q(\theta)$, respectively, where $\theta = |\vartheta|$. Both these CPDFs show power-law-scaling regions: $Q(\kappa) \sim \kappa^{-h_\kappa+1}$, for $\kappa \rightarrow \infty$,

with $h_\kappa \simeq 2.5$, i.e., the PDF $P(\kappa) \sim \kappa^{-h_\kappa}$; and $Q(\theta) \sim \theta^{-h_\theta+1}$, for $\theta \rightarrow \infty$, with $h_\theta \simeq 3$, i.e., the PDF $P(\theta) \sim \theta^{-h_\theta}$. In Figs. 6(c) and 6(d) we present, for counterflow ST, the CPDFs $Q(\kappa)$ and $Q(\theta)$, respectively. The exponents h_κ and h_θ are the same as for coflow ST. We use a local-slope analysis (see, e.g., Ref. 71) to calculate the mean values of h_κ and h_θ and their error bars [insets of Figs. 6(a) and 6(b)]. The exponents h_κ and h_θ , for the tails $P(\kappa)$ and $P(\theta)$ are universal, insofar as they are independent of $B, B', \rho_n, \rho_s, St_n, St_n,$ and \tilde{U}_{ns} . The exponents h_κ and h_θ have the same values as they do in classical fluid turbulence.^{67,72,73}

We can obtain h_κ and h_θ , by making plausible approximations, as in classical fluid turbulence.^{72,73} For the curvature

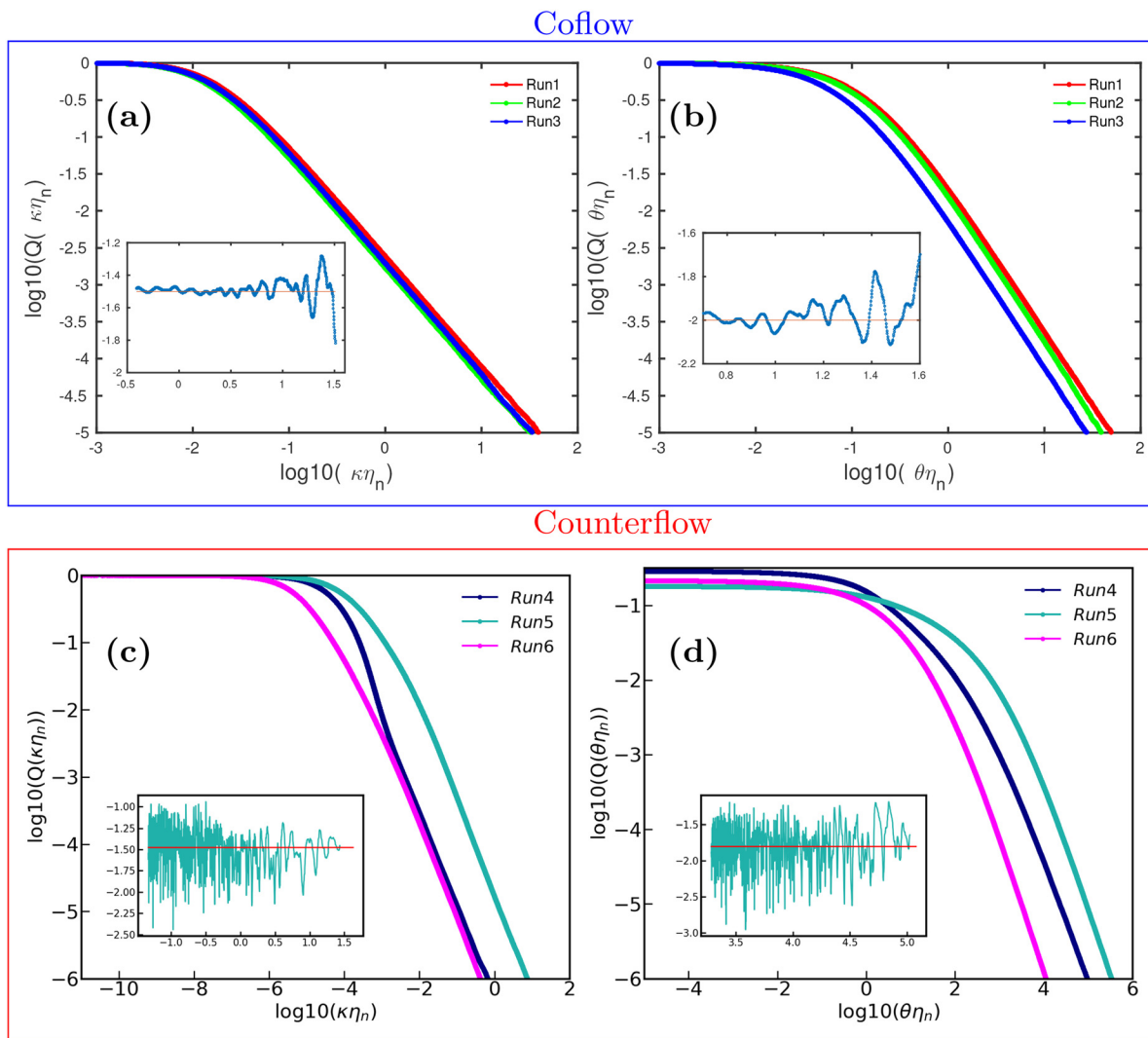


FIG. 6. Log-log plots of CPDFs of (a) the curvature κ and (b) the magnitude θ of the torsion of particle trajectories for coflow ST (runs R1, R2, and R3); (c) and (d) are, respectively, the counterflow-ST counterparts of (a) and (b) (for runs R5, R6). Insets show plots of the local slopes of the tails of these CPDFs for run R1 [in (a) and (b)] and for run R5 [in (c) and (d)]; the mean values of these local slopes yield the exponents of the power-law tail of the CPDFs (and the local-slope standard deviations give the error bars for these exponents). [We can also calculate the exponent of the tail of the CPDF of κ from the instantaneous angles of particle trajectories (see Fig. S3 in [supplementary material V](#)).] In these plots $St_n = 1.0$ and $\beta = 0.88$.

$$P(\kappa) = \int \delta\left(\kappa - \frac{a_n}{v^2}\right) \mathcal{P}(a_n, v) da_n dv, \quad (19)$$

where a_n is the normal component of the particle's acceleration, and v the magnitude of its velocity. Furthermore, $\theta = \frac{|\mathbf{v} \cdot (\dot{\mathbf{v}} \times \hat{\mathbf{v}})|}{(v \cdot \mathbf{v})^3 \kappa^2}$, which we can simplify to obtain $\theta = \frac{|\dot{\mathbf{v}} \cdot \hat{\mathbf{b}}|}{a_n v}$; large values of θ correspond to small values of a_n or v . For the modulus of the torsion

$$P(\theta) = \int \delta\left(\theta - \frac{1}{a_n v}\right) \mathcal{P}(a_n, v) da_n dv. \quad (20)$$

a_n is a small-scale quantity, and v is dominated by large-scale flows, so we argue, as in Ref. 67, that this scale separation suggests^{67,72,73} that we have the following factorization of the joint PDF:

$$\mathcal{P}(a_n, v) \simeq P_{a_n}(a_n) P_v(v). \quad (21)$$

From our DNSs of the 3D HVBK model, we find that: (a) the PDF of v is well approximated by the Maxwellian

$$P_v(v) = C_1 v^{d-1} \exp(-v^2/C_2), \quad (22)$$

where C_1 and C_2 do not depend on v ; and (b) the PDF of a_n can be fit to the form

$$P_{a_n}(a_n) = C_3 a_n \exp(-a_n^2/C_4), \quad (23)$$

where C_3 and C_4 do not depend on a_n . By substituting Eqs. (21)–(23) in Eqs. (19) and (20), we get, after some simplification (in the small a_n limit),

$$\begin{aligned} P(\kappa) &\sim \kappa^{-2.5}, & \kappa \rightarrow \infty, \\ P(\theta) &\sim \theta^{-3}, & \theta \rightarrow \infty, \end{aligned} \quad (24)$$

our DNS results are in agreement with these power-law forms.

D. Energy increments and the irreversibility of 3D HVBK turbulence

We turn now to the energy increments of inertial particles advected by 3D HVBK turbulent flows

$$W(\tau) = \langle E_{(t_0+\tau)} - E_{(t_0)} \rangle_{t_0}, \quad (25)$$

where $E_t = (1/2)\mathbf{v}(t)^2$ is the kinetic energy per unit mass of the particle, and the particle velocity \mathbf{v} is calculated by using Eqs. (5); $\langle \rangle_{t_0}$

denotes the average over the time origin t_0 . Such energy increments have been used to study irreversibility in classical fluid turbulence, where it has been found that inertial particles, in turbulent flows of a classical fluid, gain energy slowly but lose it rapidly;^{76,77} such gain and loss are also referred to as flight-crash events because, on average, a particle decelerates faster than it accelerates. In Figs. 7(a) and 7(c), we plot, respectively, the PDFs $P(W/\sigma_W)$, where σ_W is the standard deviation, for coflow ST and counterflow ST at $T = 1.65$ K and for light particles ($\beta = 1.25$).

For coflow ST, we observe that $P(W/\sigma_W)$ is negatively skewed for the small values of τ , which indicates that the particles lose energy faster than they gain it. This skewness decreases as we increase τ , as we show in blue curve of Fig. 7(a) for coflow ST; clearly, these PDFs are more symmetrical (and somewhat close to Gaussian PDFs) than their small- τ counterparts in Fig. 7(a).

There is a striking difference if we consider light particles ($\beta = 1.25$) in counterflow ST [Fig. 7(c)]: the skewness of $P(W/\sigma_W)$ is positive (as has been found recently in a model for bacterial turbulence⁷⁸). We conjecture that this positive skewness arises because, in counterflow ST, the mean velocity \tilde{U}_{ns} makes light particles cluster near large vortical structures [Fig. 1(d)].

In Figs. 7(b) and 7(d), we present, for coflow ST and counterflow ST, respectively, and for different values of St_n , graphs of the scaled third moment of the energy increment $\langle W^3/E_{nf}^3 \rangle$ vs the scaled time increment τ/τ_{nf}^n , where E_{nf} and τ_{nf}^n are, respectively, the energy and the dissipation timescale for the normal fluid. From Figs. 7(b) and 7(d), we infer that this third moment is negative for coflow ST but positive for counterflow ST. For small time increments in coflow ST

$$-\langle W^3/E_{nf}^3 \rangle \sim (\tau/\tau_{nf}^n)^3, \quad (26)$$

and for counterflow ST

$$\langle W^3/E_{nf}^3 \rangle \sim (\tau/\tau_{nf}^n)^3, \quad (27)$$

deviations from these simple-scaling form are evident at large values of τ/τ_{nf}^n .

Flight-crash events have also been studied for coflow ST and thermal-counterflow ST in experiments with superfluid ⁴He, by using particles that are like Lagrangian tracers.²² These experiments find that, on scales larger than the mean inter-vortex spacing and for

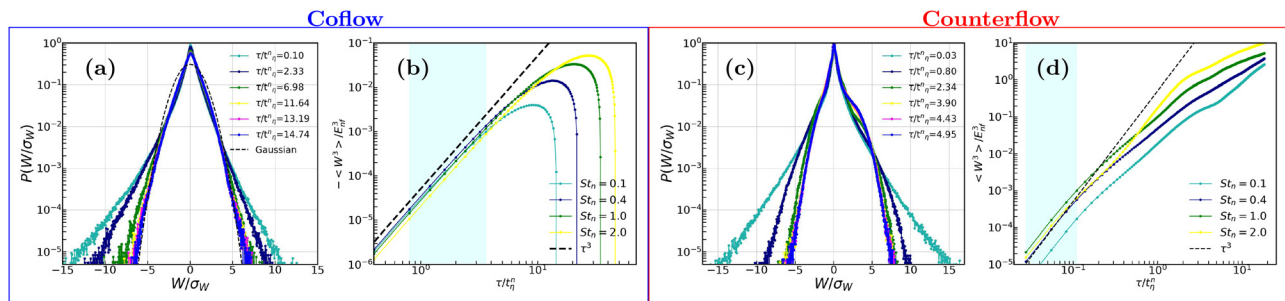


FIG. 7. Semilog plots of the energy-increment PDF $P(W/\sigma_W)$, where σ_W is the standard deviation of W , for coflow ST (columns 1–2) and for counterflow ST (columns 3–4) at $T = 1.65$ K: (a) for different time lags τ/τ_{nf}^n , where τ_{nf}^n is the normal-fluid dissipation time; (b) log–log plots of $\langle -W^3/E_{nf}^3 \rangle$ vs the time lag τ/τ_{nf}^n , where E_{nf}^n is the normal-fluid energy, and τ^3 is indicated by the black-dashed line. (c) and (d) are the counterflow-ST versions of (a) and (b), respectively. The cyan-shaded regions show the regimes over which we fit power laws. The dashed curve in (a) shows the Gaussian fits for $P(W/\sigma_W)$ for $\tau/\tau_{nf}^n = 14.74$ with 0 mean and unit standard deviation. For all the plots $St_n = 1.0$ and $\beta = 0.88$.

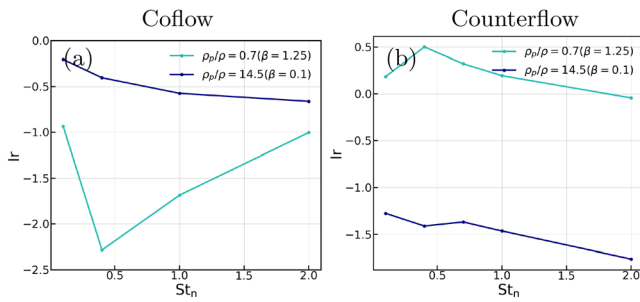


FIG. 8. Plots of the irreversibility parameter Ir (see the text) vs St_n for (a) coflow ST and (b) counterflow ST. These plots are at $T = 1.65\text{K}$ and for $\beta = 0.1$ in navy color and for $\beta = 1.25$ in light sea green.

mechanically driven coflow ST, there are negatively skewed PDFs $P(W/\sigma_W)$, which are signatures of flight-crash events (see above); these experimental results are in consonance with our findings for coflow ST [Figs. 7(a) and 7(b)]. Experiments²² have also shown that the flight-crash events are less apparent in counterflow ST than in coflow ST, and there are signatures of positively skewed velocity-difference PDFs as well; this is in agreement with our results [Figs. 7(c) and 7(d)] for light particles. Furthermore, these experiments²² find that, on scales smaller than or comparable to the mean inter-vortex spacing, there is less evidence for flight-crash events than in classical fluid turbulence; we cannot address this here because, as we have noted above, the HVBK model cannot be used for a description of superfluid turbulence on length scales smaller than or comparable to the mean inter-vortex spacing. However, even in this model of HVBK, the results of counterflow are strikingly different from that of coflow.

To quantify the irreversibility of the flow, we can calculate the power $p(t) = \mathbf{a}(t) \cdot \mathbf{v}(t)$, from particle trajectories, with $\mathbf{a} = d\mathbf{v}/dt$ being the particle’s acceleration. The irreversibility parameter is, as in classical fluid turbulence,⁷⁶

$$Ir = \frac{\langle p^3 \rangle}{\langle p^2 \rangle^{3/2}}, \quad (28)$$

which we plot vs St_n in Figs. 8(a) and 8(b) for coflow and counterflow ST, respectively, at $T = 1.65\text{K}$ and for both light and heavy particles. For coflow ST, this irreversibility parameter is negative for light ($\beta = 1.25$) as well as heavy ($\beta = 0.1$) particles and for all St_n ; this has also been found in classical fluid turbulence.⁷⁶ Moreover, it has been argued⁷⁹ that $Ir < 0$ in 3D fluid turbulence; similar arguments can be used, mutatis mutandis, to conclude that $Ir < 0$ in 3D HVBK coflow turbulence, in agreement with our graphs in Fig. 8(a). For counterflow ST, the irreversibility parameter [Fig. 8(b)] is positive for light particles ($\beta = 1.25$), which reflects the positive skewness in the energy increments of Figs. 7(c) and 7(d); in contrast, for heavy particles ($\beta = 0.1$), the irreversibility parameter is negative [navy-blue curve in Fig. 8(b)], which indicates negatively skewed PDFs of energy increments.

IV. CONCLUSIONS

Studies of inertial particles in superfluid turbulence are in their infancy; by contrast, there have been extensive studies of the statistical properties of such particles advected by classical fluid turbulence.^{38,39}

Hence, we have carried out a systematic study of inertial particles in statistically steady coflow ST and counterflow ST in the 3D HVBK model, for different values of the Stokes numbers St_n , with normal-fluid fractions and mutual-friction coefficients that are taken from measurements⁶⁰ on superfluid ⁴He, as a function of the temperature. One recent study³⁷ has investigated the clustering of inertial particles in 3D HVBK turbulence and has shown that, for coflow ST, although the particle distribution is nearly uniform at high temperatures, it still has signatures of some clustering.

Coflow ST is isotropic, but counterflow ST is inherently anisotropic; we have shown this via isosurfaces of $|\omega_n|$ and the positions of representative particles in Fig. 1. For coflow ST at $T = 1.65\text{K}$, particles cluster as they do in classical fluid turbulence because, at this temperature, the mutual friction couples both fluids strongly. The particles form large-scale clusters at $T = 1.65\text{K}$ in counterflow ST; and light particles are attracted toward [Fig. 1(d)] the large vortical columns; by contrast, heavy particles are expelled from these vortical columns [Fig. 1(c)].

These large vortical columns have a direct influence on the statistics of the angle Θ , which is the angle between subsequent inertial-particle-displacement increment. The study of Θ reveals two scaling regions; one in dissipation and other in the inertial region. In the case of coflow ST, the large time asymptotic value of Θ is the same for all Stokes numbers which is the signature of isotropic case.⁶⁵ While for counterflow, this asymptotic value of Θ reduces for light particles with large St_n as they are affected more by the confinement from normal fluid component. Reference 66 studies the effect of mean velocity on the angle Θ in the case of classical turbulence and also observe such reduction in the large time lag value of Θ .

One of the main results of this study is the signature of positive skewness in the PDFs of energy increment Figs. 7(c) and 7(d) for light particles. As we mention earlier, in a recent study of coflow and counterflow ST, Ref. 22 observes that the flight crash events are less prominent than that of classical fluid turbulence; they show that for coflow, there is some similarity to classical case at large length scales. This result of coflow is in agreement with our study, i.e., there are signatures of flight crash events in the HVBK model of coflow. For counterflow, Ref. 22 observes different results from the classical case at all length scales and found signatures of positive skewness in moments of velocity differences. This is also in consonance with our results of positive skewness in the case of counterflow for light particles; while for heavy particles, the PDFs of energy increment are negatively skewed.

We hope that our definition and study of flight crash events, for inertial particles in 3D HVBK turbulence, will lead to new experimental investigations of this problem in, e.g., superfluid ⁴He or Bose–Einstein condensates (BECs).

SUPPLEMENTARY MATERIAL

See the [supplementary material](#) for: (1) a brief description of the specific power laws found in Fig. 2; (2) isosurface plots of the magnitude of the normal-fluid vorticity $|\omega_n|$ at temperature $T = 2.10\text{K}$; (3) CPDFs of the persistence time III A, t_s^{per} , at $T = 1.65\text{K}$ for the superfluid component; (4) the curvature III C, κ , of particle trajectories, obtained from the instantaneous angle $\Theta(t, \tau)$; (5) isosurface plots of the magnitude of the normal-fluid vorticity $|\omega_n|$ at temperature $T = 2.10\text{K}$ for a square cuboid domain with resolution $256 \times 256 \times 1024$.

ACKNOWLEDGMENTS

We thank Samridhhi Sankar Ray and Kiran Kolluru for discussions, SERB and CSIR (India) for support, and the National Supercomputing Mission (NSM) and SERC (IISc) for computational resources. S.S. acknowledges support from the PMRF. V.S. acknowledges support from the Start-up Research Grant No. SRG/2020/000993 from SERB, India, Grant No. IIT/SRIC/ISIRD/2021-2022/03 from the Institute Scheme for Innovative Research and Development (ISIRD), IIT Kharagpur, and the NSM for providing computing resources of “PARAM Shakti” at IIT Kharagpur, which is implemented by C-DAC and supported by the Ministry of Electronics and Information Technology (MeitY) and the Department of Science and Technology (DST), Government of India.

AUTHOR DECLARATIONS

Conflict of Interest

The authors have no conflicts to disclose.

Author Contributions

Akhilesh Kumar Verma and Sanjay Shukla contributed equally to this study.

Sanjay Shukla: Conceptualization (equal); Data curation (equal); Formal analysis (equal); Writing – original draft (equal). **Akhilesh Kumar Verma:** Conceptualization (equal); Data curation (equal); Formal analysis (equal); Writing – original draft (equal). **Vishwanath Shukla:** Conceptualization (equal). **Akshay Bhatnagar:** Conceptualization (equal). **Rahul Pandit:** Conceptualization (equal); Formal analysis (equal); Writing – original draft (equal); Writing – review & editing (equal).

DATA AVAILABILITY

The data that support the findings of this study are available from corresponding author upon reasonable request.

NOMENCLATURE

Ir	Irreversibility
p	Power input to the particle
$Q_{n/s}, R_{n/s}$	Invariants of velocity gradient tensor for normal-fluid/superfluid
$t_{n/s}^{per}$	Persistence time of particles for normal-fluid/superfluid
$U_{ns}(\tilde{U}_{ns})$	Counterflow mean velocity (magnitude of mean relative velocity)
$W(\tau)$	Particle’s kinetic energy increment separated by time lag τ
α, ζ	exponents of the angle Θ
β	Parameter that accounts for the added mass effect to the particle
θ	Magnitude of the torsion of the particle’s trajectory
κ	Curvature of the particle’s trajectory
ρ_p	Particle’s density
$\tau_{\eta}^{n/s}$	Kolmogorov-dissipation timescale for normal fluid/superfluid
Θ	Angle between particle’s subsequent position increment

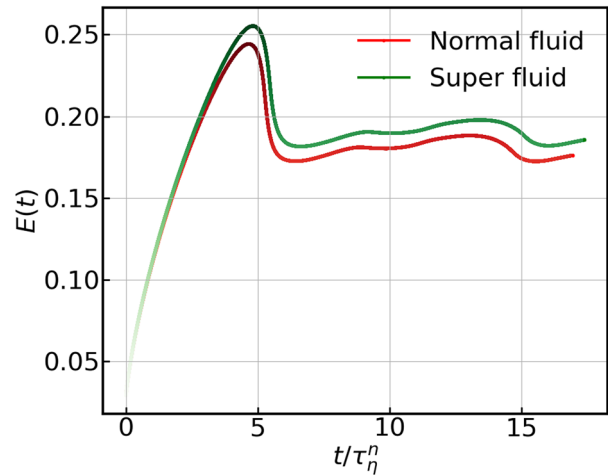


FIG. 9. Plot of the volume-averaged energy, $E(t) = \sum_{k_{\parallel}} E_{k_{\parallel}} + \sum_{k_{\perp}} E_{k_{\perp}}$, of the turbulent flow for normal fluid and superfluid components showing the statistically steady state at long times. Here, $E_{k_{\parallel}}$ and $E_{k_{\perp}}$ are defined in Eqs. (10), and τ_{η}^n is the dissipation timescale for the normal fluid.

APPENDIX: THE VOLUME-AVERAGED ENERGY

Plot of the volume-averaged energy $E(t) = \sum_{k_{\parallel}} E_{k_{\parallel}} + \sum_{k_{\perp}} E_{k_{\perp}}$, of the turbulent flow for normal fluid and superfluid components showing the statistically steady state at long times.

REFERENCES

- ¹R. A. Shaw, “Particle-turbulence interactions in atmospheric clouds,” *Annu. Rev. Fluid Mech.* **35**, 183 (2003).
- ²W. W. Grabowski and L. P. Wang, “Growth of cloud droplets in a turbulent environment,” *Annu. Rev. Fluid Mech.* **45**, 293 (2013).
- ³G. Falkovich, A. Fouxon, and M. Stepanov, “Acceleration of rain initiation by cloud turbulence,” *Nature* **419**, 151 (2002).
- ⁴P. J. Armitage, *Astrophysics of Planet Formation* (Cambridge University Press, Cambridge, 2010).
- ⁵J. Eaton and J. Fessler, “Preferential concentration of particles by turbulence,” *Int. J. Multiphase Flow* **20**, 169 (1994).
- ⁶S. Post and J. Abraham, “Modeling the outcome of drop–drop collisions in diesel sprays,” *Int. J. Multiphase Flow* **28**, 997 (2002).
- ⁷J. Cardy, G. Falkovich, and K. Gawedzki, *Non-Equilibrium Statistical Mechanics and Turbulence* (Cambridge University Press, Cambridge, 2008).
- ⁸R. J. Donnelly, *Quantized Vortices in Helium II* (Cambridge University Press, Cambridge, 1991).
- ⁹M. S. Paoletti and D. P. Lathrop, “Quantum turbulence,” *Annu. Rev. Condens. Matter Phys.* **2**, 213 (2011).
- ¹⁰L. Skrbek and K. R. Sreenivasan, “Developed quantum turbulence and its decay,” *Phys. Fluids* **24**, 011301 (2012).
- ¹¹N. G. Berloff, M. Brachet, and N. P. Proukakis, “Modeling quantum fluid dynamics at nonzero temperatures,” *Proc. Natl. Acad. Sci. U. S. A.* **111**, 4675 (2014).
- ¹²M. Tsubota, K. Fujimoto, and S. Yui, “Numerical studies of quantum turbulence,” *J. Low Temp. Phys.* **188**, 119 (2017).
- ¹³C. F. Barenghi and N. G. Parker, *A Primer on Quantum Fluids*, SpringerBriefs on Physics (Springer, 2017).
- ¹⁴G. P. Bewley, D. P. Lathrop, and K. R. Sreenivasan, “Visualization of quantized vortices,” *Nature* **441**, 588 (2006).
- ¹⁵G. P. Bewley, M. S. Paoletti, K. R. Sreenivasan, and D. P. Lathrop, “Characterization of reconnecting vortices in superfluid helium,” *Proc. Natl. Acad. Sci. U. S. A.* **105**, 13707 (2008).

- ¹⁶D. R. Poole, C. F. Barenghi, Y. A. Sergeev, and W. F. Vinen, "Motion of tracer particles in He II," *Phys. Rev. B* **71**, 064514 (2005).
- ¹⁷M. L. Mantia, D. Duda, M. Rotter, and L. Skrbek, "Lagrangian accelerations of particles in superfluid turbulence," *J. Fluid Mech.* **717**, R9 (2013).
- ¹⁸M. L. Mantia and L. Skrbek, "Quantum turbulence visualized by particle dynamics," *Phys. Rev. B* **90**, 014519 (2014).
- ¹⁹D. E. Zmeev, F. Pakpour, P. M. Walmsley, A. I. Golov, W. Guo, D. N. McKinsey, G. G. Ihas, P. V. E. McClintock, S. N. Fisher, and W. F. Vinen, "Excimers He₂* as tracers of quantum turbulence in ⁴He in the T=0 limit," *Phys. Rev. Lett.* **110**, 175303 (2013).
- ²⁰W. Guo, M. L. Mantia, D. P. Lathrop, and S. W. V. Sciver, "Visualization of two-fluid flows of superfluid helium-4," *Proc. Natl. Acad. Sci. U. S. A.* **111**, 4653–4658 (2014).
- ²¹Y. Tang, S. Bao, T. Kanai, and W. Guo, "Statistical properties of homogeneous and isotropic turbulence in He II measured via particle tracking velocimetry," *Phys. Rev. Fluids* **5**, 084602 (2020).
- ²²P. Švančara and M. L. Mantia, "Flight-crash events in superfluid turbulence," *J. Fluid Mech.* **876**, R2 (2019).
- ²³G. Krstulovic and M. Brachet, "Energy cascade with small-scale thermalization, counterflow metastability, and anomalous velocity of vortex rings in Fourier-truncated Gross-Pitaevskii equation," *Phys. Rev. E* **83**, 066311 (2011).
- ²⁴V. Shukla, M. Brachet, and R. Pandit, "Turbulence in the two-dimensional Fourier-truncated Gross-Pitaevskii equation," *New J. Phys.* **15**, 113025 (2013).
- ²⁵E. Zaremba, T. Nikuni, and A. Griffin, "Dynamics of trapped Bose gases at finite temperatures," *J. Low Temp. Phys.* **116**, 277 (1999).
- ²⁶T. Winiecki and C. S. Adams, "Motion of an object through a quantum fluid," *Europhys. Lett.* **52**, 257 (2000).
- ²⁷V. Shukla, M. Brachet, and R. Pandit, "Sticking transition in a minimal model for the collisions of active particles in quantum fluids," *Phys. Rev. A* **94**, 041602 (2016).
- ²⁸V. Shukla, R. Pandit, and M. Brachet, "Particles and fields in superfluids: Insights from the two-dimensional Gross-Pitaevskii equation," *Phys. Rev. A* **97**(1), 013627 (2018).
- ²⁹U. Giuriato and G. Krstulovic, "Interaction between active particles and quantum vortices leading to Kelvin wave generation," *Sci. Rep.* **9**(1), 4839 (2019).
- ³⁰U. Giuriato, G. Krstulovic, and D. Proment, "Clustering and phase transitions in a 2D superfluid with immiscible active impurities," *J. Phys. A* **52**, 305501 (2019).
- ³¹U. Giuriato, G. Krstulovic, and S. Nazarenko, "How do trapped particles interact with and sample superfluid vortex excitations?," [arXiv:1907.01111v1](https://arxiv.org/abs/1907.01111v1) (2019).
- ³²L. Biferale, D. Khomenko, V. L'vov, A. Pomyalov, I. Procaccia, and G. Sahoo, "Superfluid helium in three-dimensional counterflow differs strongly from classical flows: Anisotropy on small scales," *Phys. Rev. Lett.* **122**, 144501 (2019).
- ³³D. Khomenko, V. S. L'vov, A. Pomyalov, and I. Procaccia, "Counterflow-induced decoupling in superfluid turbulence," *Phys. Rev. B* **93**, 014516 (2016).
- ³⁴J. I. Polanco and G. Krstulovic, "Counterflow-induced inverse energy cascade in three-dimensional superfluid turbulence," *Phys. Rev. Lett.* **125**, 254504 (2020).
- ³⁵V. S. L'vov, Y. V. Lvov, S. Nazarenko, and A. Pomyalov, "Theory of anisotropic superfluid ⁴He counterflow turbulence," [arXiv:2106.07014](https://arxiv.org/abs/2106.07014) (2021).
- ³⁶C. F. Barenghi, L. Skrbek, and K. R. Sreenivasan, "Introduction to quantum turbulence," *Proc. Natl. Acad. Sci.* **111**, 4647–4652 (2014).
- ³⁷J. I. Polanco and G. Krstulovic, "Inhomogeneous distribution of particles in coflow and counterflow quantum turbulence," *Phys. Rev. Fluids* **5**, 032601(R) (2020).
- ³⁸F. Toschi and E. Bodenschatz, "Lagrangian properties of particles in turbulence," *Annu. Rev. Fluid Mech.* **41**, 375 (2009).
- ³⁹J. Bec, "Multifractal concentrations of inertial particles in smooth random flows," *J. Fluid Mech.* **528**, 255 (2005).
- ⁴⁰R. J. Donnelly, "Cryogenic fluid dynamics," *J. Phys.* **11**, 7783 (1999).
- ⁴¹C. F. Barenghi, R. J. Donnelly, and W. F. Vinen, "Friction on quantized vortices in helium II. A review," *J. Low Temp. Phys.* **52**, 189 (1983).
- ⁴²H. E. Hall and W. F. Vinen, "The rotation of liquid helium II. The theory of mutual friction in uniformly rotating helium II," *Proc. R. Soc. London, Ser. A* **238**, 215 (1956).
- ⁴³I. M. Khalatnikov, *An Introduction to the Theory of Superfluidity* (W. A. Benjamin, New York, 1965).
- ⁴⁴P. E. Roche, C. F. Barenghi, and E. Lévéque, "Quantum turbulence at finite temperature: The two-fluids cascade," *Europhys. Lett.* **87**, 54006 (2009).
- ⁴⁵V. Shukla, A. Gupta, and R. Pandit, "Homogeneous isotropic superfluid turbulence in two dimensions: Inverse and forward cascades in the Hall-Vinen-Bekharevich-Khalatnikov model," *Phys. Rev. B* **92**, 104510 (2015).
- ⁴⁶L. Biferale, D. Khomenko, V. L'vov, A. Pomyalov, I. Procaccia, and G. Sahoo, "Turbulent statistics and intermittency enhancement in coflowing superfluid ⁴He," *Phys. Rev. Fluids* **3**, 024605 (2018).
- ⁴⁷A. K. Verma, V. Shukla, A. Basu, and R. Pandit, "The statistical properties of superfluid turbulence in ⁴He from the Hall-Vinen-Bekharevich-Khalatnikov model," [arXiv:1905.01507](https://arxiv.org/abs/1905.01507) (2019).
- ⁴⁸W. F. Vinen, "Mutual friction in a heat current in liquid helium II III. Theory of the mutual friction," *Proc. R. Soc. London, Ser. A* **242**, 493 (1957).
- ⁴⁹F. Toschi, L. Biferale, G. Boffeta, A. Celani, B. J. Devenish, and A. Lanotte, "Acceleration and vortex filaments in turbulence," *J. Turbul.* **6**, N15 (2005).
- ⁵⁰L. Biferale, G. Boffeta, A. Celani, A. Lanotte, and F. Toschi, "Particle trapping in three-dimensional fully developed turbulence," *Phys. Fluids* **6**, 15 (2005).
- ⁵¹W. F. Vinen and J. J. Niemela, "Quantum turbulence," *J. Low Temp. Phys.* **128**(5–6), 167–231 (2002).
- ⁵²V. S. L'vov, S. V. Nazarenko, and O. Rudenko, "Bottleneck crossover between classical and quantum superfluid turbulence," *Phys. Rev. B* **76**, 024520 (2007).
- ⁵³K. Morris, J. Koplik, and D. W. I. Rouson, "Vortex locking in direct numerical simulations of quantum turbulence," *Phys. Rev. Lett.* **101**, 015301 (2008).
- ⁵⁴D. H. Wacks and C. F. Barenghi, "Shell model of superfluid turbulence," *Phys. Rev. B* **84**, 184505 (2011).
- ⁵⁵C. Canuto, M. Y. Hussaini, A. Quarteroni, and T. A. Zang, *Spectral Methods in Fluid Dynamics* (Springer-Verlag, Berlin, 1988).
- ⁵⁶D. Gottlieb and S. A. Orszag, *Numerical Analysis of Spectral Methods* (SIAM, Philadelphia, 1977).
- ⁵⁷See <https://www.fftw.org/> for a guide to the FFTW package for Fast Fourier Transforms.
- ⁵⁸A. G. Lamorgese, D. A. Caughey, and S. B. Pope, "Direct numerical simulation of homogeneous turbulence with hyperviscosity," *Phys. Fluids* **17**, 015106 (2005).
- ⁵⁹G. Sahoo, P. Perlekar, and R. Pandit, "Systematics of the magnetic-Prandtl-number dependence of homogeneous, isotropic magnetohydrodynamic turbulence," *New J. Phys.* **13**, 013036 (2011).
- ⁶⁰R. J. Donnelly and C. F. Barenghi, "The observed properties of liquid helium at the saturated vapor pressure," *J. Phys. Chem. Ref. Data* **27**, 1217 (1998).
- ⁶¹L. Boué *et al.*, "Energy and vorticity spectra in turbulent superfluid ⁴He from T=0 to T_λ," *Phys. Rev. B* **91**, 144501 (2015).
- ⁶²R. Gagnon, "The Faxén formulas for a rigid particle in an unsteady non-uniform stokes-flow," *J. Méc. Théor. Appl.* **2**, 143 (1983).
- ⁶³M. R. Maxey and J. J. Riley, "Equation of motion for a small rigid sphere in a nonuniform flow," *Phys. Fluids* **26**, 883–889 (1983).
- ⁶⁴J. Bec *et al.*, "Lyapunov exponents of heavy particles in turbulence," *Phys. Fluids* **18**, 091702 (2006).
- ⁶⁵W. J. T. Bos, B. Kadoch, and K. Schneider, "Angular statistics of Lagrangian trajectories in turbulence," *Phys. Rev. Lett.* **114**, 214502 (2015).
- ⁶⁶X. He, S. Apte, K. Schneider, B. Kadoch, and M. Farge, "Center for turbulence research" *Proc. Summer Prog.* **18**, 113047 (2016).
- ⁶⁷A. Bhatnagar, A. Gupta, D. Mitra, P. Perlekar, M. Wilkinson, and R. Pandit, "Deviation-angle and trajectory statistics for inertial particles in turbulence," *Phys. Rev. E* **94**, 063112 (2016).
- ⁶⁸M. Spivak, *A Comprehensive Introduction to Differential Geometry* (Publish or Perish, Boston, MA, 1970), Vol. 1–5.
- ⁶⁹M. Stone and P. Goldbart, *Mathematics for Physics: A Guided Tour for Graduate Students* (Cambridge University Press, 2009), p. 242.
- ⁷⁰W. Braun, F. D. Lillo, and B. Eckhardt, "Geometry of particle paths in turbulent flows," *J. Turbul.* **7**, 1 (2006).
- ⁷¹P. Perlekar, S. S. Ray, D. Mitra, and R. Pandit, "Persistence problem in two-dimensional fluid turbulence," *Phys. Rev. Lett.* **106**, 054501 (2011).
- ⁷²H. Xu, N. T. Ouellette, and E. Bodenschatz, "Curvature of Lagrangian trajectories in turbulence," *Phys. Rev. Lett.* **98**, 050201 (2007).
- ⁷³A. Scagliarini, "Geometric properties of particle trajectories in turbulent flows," *J. Turbul.* **12**, N25 (2011).

- ⁷⁴A. Bhatnagar, A. Gupta, D. Mitra, R. Pandit, and P. Perlekar, “How long do particles spend in vortical regions in turbulent flows?,” *Phys. Rev. E* **94**, 053119 (2016).
- ⁷⁵R. Gomes-Fernandes, B. Ganapathisubramani, and J. Vassilicos, “Evolution of the velocity-gradient tensor in a spatially developing turbulent flow,” *J. Fluid Mech.* **756**, 252–292 (2014).
- ⁷⁶A. Bhatnagar, A. Gupta, D. Mitra, and R. Pandit, “Heavy inertial particles in turbulent flows gain energy slowly but lose it rapidly,” *Phys. Rev. E* **97**, 033102 (2018).
- ⁷⁷H. Xu, A. Pumir, G. Falkovich, E. Bodenschatz, M. Shats, H. Xia, N. Francois, and G. Boffetta, “Flight-crash events in turbulence,” *Proc. Natl. Acad. Sci. U. S. A.* **111**, 7558 (2014).
- ⁷⁸K. V. Kiran *et al.*, “Irreversibility in bacterial turbulence: Insights from the mean-bacterial-velocity model,” [arXiv:2201.12722](https://arxiv.org/abs/2201.12722) (2022).
- ⁷⁹A. Pumir, H. Xu, E. Bodenschatz, and R. Grauer, “Single-particle motion and vortex stretching in three-dimensional turbulent flows,” *Phys. Rev. Lett.* **116**, 124502 (2016).